

Electronic Structure Calculation of Muonium in Silicon

メタデータ	言語: eng 出版者: 公開日: 2020-01-08 キーワード (Ja): キーワード (En): 作成者: メールアドレス: 所属:
URL	http://hdl.handle.net/2297/00056472

This work is licensed under a Creative Commons Attribution-NonCommercial-ShareAlike 3.0 International License.



KANAZAWA UNIVERSITY

DISSERTATION

**Electronic Structure Calculation of Muonium in
Silicon**

シリコン中ミュオニウムの電子構造計算

Author:

Muhamad Nasruddin Manaf
1624012012

Supervisor:

Prof. Mineo Saito

*A thesis submitted in fulfilment of the requirements
for the degree of Doctor of Philosophy in Science*

in the

Division of Mathematical and Physical Sciences
Graduate School of Natural Science and Technology
Kanazawa University

June, 2019

KANAZAWA UNIVERSITY

Abstract

Division of Mathematical and Physical Sciences
Graduate School of Natural Science and Technology

Doctor of Philosophy in Science

Electronic Structure Calculation of Muonium in Silicon

by Muhamad Nasruddin Manaf

We present calculations of the electronic structure of muonium in silicon, in particular, muonium at the bond center (BC) site. Muonium at the BC site in silicon is commonly recognized as anomalous muonium (AM) due to the fact that the spin density at muonium site has a negative value instead of a positive one. The spin density corresponds to experimentally observed parameter which is recognized as Fermi Contact Interaction Constant (FCIC). Previous studies reported the result of first-principles calculations. However, the FCIC shows significant deviations from the experimental value. The origin of the negative value of FCIC has not been explained yet. Therefore, in this study, we present reliable calculations to get reliable results. We calculate AM in silicon using spin-polarized density functional theory based on general gradient approximation or local density approximation. We carry out accurate calculations of the FCIC by increasing the size of supercell. The disagreement between the previously reported values and the experimental one is found to be the sizes of the supercells, which is not sufficient: the distance between muoniums is too small due to the small sizes of the supercells. Therefore, the effect of interaction between muoniums can not be excluded. We also clarify that the origin of the negative value of FCIC is the correlation effect. By considering the Hubbard model of linear three-hydrogen molecule, we find the correlation effect induces the negative FCIC value at muonium site. On the other hand, the FCIC is zero when we do not include the correlation effect.

Keywords: silicon, muonium, supercells and electron correlation effect

Acknowledgements

First of all, I would like to express my gratitude to Professor Mineo Saito as my supervisor for his suggestion, guidance and encouragement during supervising me as a Doctoral Student at Kanazawa University. I give my highest appreciation to Associate Professor Fumiyuki Ishii, Dr. Sholihun, Mr. Susumu Minami, Mr. Naoya Yamaguchi, Mr. Rifky Syariati and Mr. Muhammad Yusuf Hakim Widiyanto due to the valuable discussion and all supports during my time in the Kanazawa University. I also want to express my gratitude to Professor Hidemi Nagao, Professor Tatsuki Oda and Professor Shinichi Miura due to their valuable suggestions, which improve the quality of this dissertation. And also I express my gratitude to all member of The Indonesian Student Association (PPI) who always supports me. I gratefully acknowledge a scholarship from Ministry of Education, Culture, Sports, Science and Technology of Japan.

Contents

Abstract	i
Acknowledgements	ii
Contents	iii
List of Figures	v
List of Tables	vii
1 Introduction	1
1.1 Background	1
1.2 Purposes of This Study	3
1.3 Outline of Thesis	3
2 Theoretical Background	4
2.1 Schrödinger Equation and Born-Oppenheimer Approximation	4
2.2 The Variation Principle	6
2.3 Hartree-Fock Approximation	8
2.4 Density Functional Theory (DFT)	10
2.4.1 Hohenberg-Kohn Theorems	10
2.4.2 The Kohn-Sham Equation	12
2.5 Hubbard Model	16
2.6 The Calculation Methods	16
2.6.1 Spin-polarized density functional calculations	16
2.6.2 Fermi contact interaction	17
3 First-Principles Study of Anomalous Muonium in Silicon	19
3.1 Introduction	19
3.2 Results and Discussion	21
4 Summary	31
4.1 Conclusion	31

4.2 Future Scope	31
----------------------------	----

Bibliography	33
---------------------	-----------

List of Figures

2.1	Self consistent scheme of Kohn-Sham equation.	15
3.1	Geometries of pristine silicon (a) and muonium impurity at the BC site (b). $\theta_0 = 109.5^\circ$ and $l_0=2.35 \text{ \AA}$ respectively. The silicon and muonium atoms are denoted by the light brown sphere and black sphere, respectively.	20
3.2	(a) Calculated $\tilde{\eta}$ given in Eq.(7). The black solid line represents η in Eq. (2.64) deduced from experimental data[25]. We present the fitting curves for the LDA and GGA calculational results.	22
3.3	DOS (a) and PDOS of the nearest silicon atoms (b) and of the muonium (c). The vertical dashed lines indicate the Fermi level in the supercell calculations.	24
3.4	(a) Spin density where the absolute value of the isosurfaces is $1.50 \times 10^{-3} \text{ bohr}^{-3}$. The positive and negative spin densities are represented by red and green colors, respectively. The spin density was drawn using VESTA [54,55]. (b) Wavefunction of the impurity level. The red and blue colors represent positive and negative values, respectively. (c and d) Schematic view of two muonium related wavefunctions. The red and the blue colors represent the positive and negative values, respectively.	25
3.5	Spin densities of the linear tri-hydrogen molecule (the red and the green colors represent positive and negative value of isosurfaces, respectively) for the cases of $l_{H-H} = 0.82 \text{ \AA}$ (the isosurface value is $9.11 \times 10^{-2} \text{ spin/bohr}^{-3}$), $l_{H-H} = 0.95 \text{ \AA}$ (the isosurface value is $4.11 \times 10^{-2} \text{ spin/bohr}^{-3}$), and $l_{H-H} = 2.0 \text{ \AA}$ (the isosurface value is $4.11 \times 10^{-2} \text{ spin/bohr}^{-3}$). We also show the magnetic moment at each site calculated based on the Hubbard model. Two limiting cases ($t \gg U$ and $t \ll U$) are considered.	26
3.6	Schematic diagram of energies of the linear tri-hydrogen molecule on the lefthand side and wavefunctions on the righthand side where the red and blue colors represent positive and negative amplitudes, respectively.	27
3.7	(a) Spin density of the linear tri-hydrogen molecule. We carry out calculations by changing the bond length from the equilibrium bond length ($l_{H-H} = 0.95 \text{ \AA}$) (b) FCIC of anomalous muonium in silicon. The calculations are performed by changing the bond length from the equilibrium one ($l_{Si-Mu} = 1.61 \text{ \AA}$).	28

3.8	The magnetic moment of electrons based on the Hubbard model of three linear hydrogen molecule.	29
-----	--	----

List of Tables

3.1	Calculated geometry (angle) of the muonium impurity at the bond-centered (BC) site. The explanation of the geometrical parameters are given in Fig. 3.1.	21
3.2	Calculated geometry (distance between atoms) of the muonium impurity at the bond-centered (BC) site. The explanation of the geometrical parameters are given in Fig. 3.1.	21
3.3	Fitting parameters in Eq. (3.1) and Eq. (3.2)	23
3.4	FCIC of muonium at the BC site. We show our calculational results for the 512, 1000, 1728 supercells and the value of FCIC from fitting is estimated by using Eq. (3.1).	23

This thesis is dedicated to my parents.

For their love, support and encouragement

Chapter 1

Introduction

1.1 Background

Semiconductor materials have been widely used for modern devices such as light emitting diodes (LED) and transistors. Pristine semiconductors, which are commonly recognized as an intrinsic semiconductors have no useful applications. Meanwhile, defects and impurities can modify the electronic properties and increase the carrier concentration of the electron or hole; and enable fabrication of n-type and p-type semiconductors. The n-type and p-type semiconductors are commonly recognized as a extrinsic semiconductors. The extrinsic semiconductors are valuable and applicable for electronic devices; for example in 2014, Shuji Nakamura, Isamu Akasaki and Hiroshi Amano won the noble prize due to the invention of the blue LED which is the breakthrough for the achievement of white LED; the lighting with the low and efficient consumption of energy[1-8]. They succeeded in fabricating the p-type gallium nitride (GaN); which was practically difficult to be achieved. They achieved the p-type GaN by using magnesium as a dopant and eliminated hydrogen impurities. Therefore, the study of defect and impurities in materials is essential.

Silicon has been studied for the last few decades. Silicon has a vital impact for the development of the transistors; this corresponds to the central part of the processor in the personal computer. Although recently developed of 2D materials have a potential to be applied for the semiconductor industry, the transistor made from bulk semiconductors have more benefits due to low-cost production. The history of a transistor was started in 1947; the germanium point-contact transistor was

invented[9]. Several years later a silicon-based transistor was launched. Then, the silicon replaced the germanium as a material for transistor due to the fact that silicon can work at room temperatures, whereas germanium transistors operate in low temperatures. The development of metal oxide semiconductors field effect transistor (MOSFET) follows the pattern of Moore's Law. Silicon is a semiconductor that is commonly used for MOSFET. Recently, the development of MOSFET has been growing so fast. This achievement is due to the reduction of the scale of the transistor into the nanometer size.

Important impurities in semiconductors are hydrogen[10]. The hydrogen atom as an impurity in materials can induce favorable or unfavorable effects due to its electronic properties. Therefore, the study of hydrogen in materials sciences has been attracting a lot of interest. In wide band-gap semiconductors such as ZnO and GaN, hydrogen may activate the shallow impurities, which can be considered as a favorable effect[10-14]. Recently, some reports explain that shallow impurities are promising for the proposal of quantum computing[15,16]. On the other hand, hydrogen also can behave as a deep donor, which is classified as an unfavorable effect[10]. Electron Paramagnetic Resonance (EPR) is one of the useful tools to study the dynamics of hydrogen. Another method that can predict the dynamics of hydrogen is muon spin resonance or commonly abbreviated as μ SR, which is one of the promising tools[17,18]. Instead of using hydrogen, μ SR uses muonium, which is a particle that mimics hydrogen and consists of sub-particles muon and electron. Muon has the same electric charge as a proton. Even though the mass is 1/9 that of the proton, the behavior of muon is similar to the proton. When muonium is implanted into the material, the muon decays into a positron, which can be detected. The information about the dynamics of muonium in materials can be extracted from the detected positron. Therefore, μ SR has been used for several decades to determine the dynamics of hydrogen in materials sciences in particular semiconductors. In μ SR, hyperfine parameters (HP), in particular, the Fermi contact interaction constants (FCIC) are observed. Analysis of these parameters gives useful information; for example, it provides information on the site of muonium, which is expected to be the stable site of hydrogen.

1.2 Purposes of This Study

The muonium in silicon is the benchmark for the study of muonium in semiconductors [22-34]. It has been recognized that the muonium in silicon can be located at bond-center or in the tetrahedral site; commonly recognized as an anomalous muonium and normal muonium, respectively. The anomalous muonium already observed in experiments[25]. Unfortunately, the accurate and the reliable theoretical calculations have not been conducted, in particular in the case of anomalous muonium. Therefore in this study we provide reliable calculation and explain the origin of the small absolute value and negative sign of FCIC at muonium site which is considered to be an unresolved problem.

We carry out first-principles calculations of muonium in silicon using density functional theory (DFT). In this thesis we focus on the study of the hyperfine parameters, in particular FCIC. We try to determine the calculation parameters and vary the size of supercells, so that we try to increase the accuracy of the calculation and can reproduce the experimental data which has not been achieved in the previous reports[29,30,33]. We explain the origin of small absolute and negative value of FCIC in the case of anomalous muonium in silicon, which is considered to be an unresolved problem. We use the Hubbard model to analyze three linear hydrogen in purposed to explain the origin of the small and negative values in anomalous muonium, and discuss possibility that the electron correlation is the origin of the negative value.

1.3 Outline of Thesis

This thesis consists of four chapters. In Chapter I, the background of this research is introduced. Then we explain some fundamental concepts of DFT in chapter II. In Chapter III, we explain the first-principles study of an anomalous muonium in silicon. We explain the origin of the small absolute and negative value of FCIC . We successfully explained that the small and negative value are due to the electron correlation. We use Hubbard model of linear three hydrogen molecule to explain this phenomena. In the last Chapter which is Chapter IV we explain the summary of our research.

Chapter 2

Theoretical Background

In this chapter, we briefly present some theory, which is related to the fundamental concepts of DFT and Hyperfine Structure (HS), in particular Fermi Contact Interaction Constant (FCIC). Firstly, we give a brief explanation of DFT from the section 2.1 to the section 2.4. We also explain the Hubbard model in section 2.5 due to the fact that the origin of small and negative value of FCIC comes from the electron correlation effect. The method to calculate HS, in particular FCIC will be explained in section 2.6.

2.1 Schrödinger Equation and Born-Oppenheimer Approximation

A full interaction of a Schrödinger eigenvalue equation for the complex system which is involving many-body interactions between electrons and nuclei can be expressed as follow:

$$\hat{H}\Psi(\mathbf{r}_1, \mathbf{R}_1, \mathbf{r}_2, \mathbf{R}_2, \dots) = E\Psi(\mathbf{r}_1, \mathbf{R}_1, \mathbf{r}_2, \mathbf{R}_2, \dots), \quad (2.1)$$

where \hat{H} and E are represent Hamiltonian and the eigenvalue respectively. The wave function Ψ has dependent with two variables, which are r_i and R_j ; where r_i and R_j represent the positions of i-th electron and j-th nucleus in the real space, respectively. The Hamiltonian operator in the Eq.(2.1) above can be expressed as below:

$$\hat{H} = \hat{T}_e + \hat{T}_n + \hat{V}_{ee} + \hat{V}_{nn} + \hat{V}_{en}, \quad (2.2)$$

where \hat{T}_e is the kinetic energy operator of the electrons, \hat{T}_n is the kinetic energy operator of the nucleus, \hat{V}_{ee} is the energy operator of electron-electron interaction, \hat{V}_{nn} is the energy operator of nucleus-nucleus interaction and \hat{V}_{en} is the energy operator of electron-nucleus interaction. The Hamiltonian above (Eq. (2.2)) consists of two parts which is classified as the kinetic energy operator and the interaction energy part. The kinetic energy part which are represented by \hat{T}_e and \hat{T}_n can be expressed as below:

$$\hat{T}_e = -\frac{1}{2} \sum_{i=1}^N \nabla_i^2(r_i), \quad (2.3)$$

and

$$\hat{T}_n = -\frac{1}{2} \sum_{j=1}^N \frac{1}{M_j} \nabla_j^2(R_j), \quad (2.4)$$

where M_j is the mass of j-th nucleus. The interaction energy operator are expressed by \hat{V}_{ee} , \hat{V}_{nn} and \hat{V}_{en} which are can be expressed as follow:

$$\hat{V}_{ee} = \frac{1}{2} \sum_{i \neq j} \frac{1}{|\mathbf{r}_i - \mathbf{r}_j|}, \quad (2.5)$$

$$\hat{V}_{nn} = \frac{1}{2} \sum_{i \neq j} \frac{Z_i Z_j}{|\mathbf{R}_i - \mathbf{R}_j|}, \quad (2.6)$$

and

$$\hat{V}_{en} = -\sum_{i,j} \frac{Z_j}{|\mathbf{r}_i - \mathbf{R}_j|}, \quad (2.7)$$

where Z_j is the atomic number. The equation (2.1) is defined by $3M+3N$ parameter in real space and it is a complex equation which is hardly solve.

By considering the significant difference of mass between electron and nucleus in which as a consequence that we can neglect the motion of the nucleus; remove the \hat{T}_n and the \hat{V}_{nn} , then the Hamiltonian in the Eq.(2.2) can be simplified as follow:

$$\hat{H} = \hat{T}_e + \hat{V}_{ee} + \hat{V}_{en}. \quad (2.8)$$

The Schrödinger equation then can be expressed as follow:

$$\hat{H}\Psi = \left[-\frac{1}{2} \sum_{i=1}^N \nabla_i^2(r_i) + \frac{1}{2} \sum_{i \neq j} \frac{1}{|\mathbf{r}_i - \mathbf{r}_j|} - \sum_{i,j} \frac{Z_j}{|\mathbf{r}_i - \mathbf{R}_j|} \right] \Psi = E\Psi. \quad (2.9)$$

This approximation is called Born-Oppenheimer approximation. This approximation can be adapted to solve from simple problem such as hydrogen atom to the problem for complex system such as bulk materials and surface. Even though the Eq.(2.9) is simple compare with the Eq. (2.1), however this equation is still hard to solve. Therefore we can reduce our problem for finding solution of the ground states. Consequently, we have to introduce additional approximation which is commonly recognized as a variation principle and Hatree-Fock approximation.

2.2 The Variation Principle

It is really hard to find the eigenfunction of the Hamiltonian for the complex system which is involving a many body interaction. Even though, we can use the trial many body interaction of eigenfunction that we have already known. Therefore, we can use the trial wavefunction with the same number electron and we can expand it in the Eq. (2.10) with the assumption that this eigenfunction is complete:

$$|\Psi\rangle = \sum_{i=1} c_i |\phi_i\rangle, \quad (2.10)$$

where c_i are the expansion coefficients and the eigenstates ϕ_i are assumed to be orthonormal. The wavefunction (Eq.(2.10)) is assume to be normalized, therefore the expectation value for the energy is given by the equation below:

$$\begin{aligned} E &= \langle \Psi | \hat{H} | \Psi \rangle \\ &= \sum_{i,j} c_j^* c_i \langle \phi_j | \hat{H} | \phi_i \rangle \\ &= \sum_i |c_i|^2 E_i \\ &\geq E_0 \sum_i |c_i|^2 = E_0. \end{aligned} \quad (2.11)$$

where E_0 is the minimum energy which is commonly recognized as the ground state energy. The expectation value of the energy of the trial wavefunction can be higher or equal with the ground state energy. Then equation (2.11) exhibit the important information which is we can find the ground state by using some trial wavefunctions. The computational cost of the calculation to find the ground state wavefunction by using trial wavefunction is depend on the accuracy of the trial

wavefunction. If the trial wavefunction is relatively close to the real wavefunction, it will reduce the computational cost.

The trial wavefunction for a given system can be expressed as a particular set of a plane wave, in which we can express as below:

$$\phi = \sum_j^N c_j \exp(-i\mathbf{k} \cdot \mathbf{r}_j), \quad (2.12)$$

The trial wavefunction above (Eq.(2.12)) should has normalized and due to the ground state energy, the wavefunction must satisfies the minimum condition:

$$\frac{\partial}{\partial c_j^*} \langle \phi | \hat{H} | \phi \rangle = 0, \quad (2.13)$$

for all c_j . Then we can introduce a new parameter which is by introducing a new quantity as follow:

$$K = \langle \phi | \hat{H} | \phi \rangle - \lambda [\langle \phi | \phi \rangle - 1]. \quad (2.14)$$

Minimizing Eq. (2.14) with respect to c_j and λ , than we can obtain

$$\frac{\partial K}{\partial c_j^*} = \frac{\partial K}{\partial \lambda} = 0, \quad (2.15)$$

where λ is called Langrange Multiplier. By inserting Eq. (2.12) to Eq. (2.14) than we can obtain

$$\sum_j c_j \left(\langle \exp(-i\mathbf{k} \cdot \mathbf{r}_i) | \hat{H} | \exp(-i\mathbf{k} \cdot \mathbf{r}_j) \rangle - \lambda \langle \exp(-i\mathbf{k} \cdot \mathbf{r}_i) | \exp(-i\mathbf{k} \cdot \mathbf{r}_j) \rangle \right) = 0. \quad (2.16)$$

Then we can write the eigenvalue equation as follow:

$$\sum_j H_{ij} c_j = \lambda \delta_{ij}, \quad (2.17)$$

where $H_{ij} = \langle \exp(-i\mathbf{k} \cdot \mathbf{r}_i) | \hat{H} | \exp(-i\mathbf{k} \cdot \mathbf{r}_j) \rangle$ and $\delta_{ij} = \langle \exp(-i\mathbf{k} \cdot \mathbf{r}_i) | \exp(-i\mathbf{k} \cdot \mathbf{r}_j) \rangle$, respectively. We can solve this equation with ($j = 1, 2, \dots, N$) by calculating the matrix element H_{ij} and δ_{ij} . By multiplying Eq. (2.17) with c_i^* and summing over j , we can get the expression below:

$$\lambda = \frac{\sum_{i,j} c_i^* c_j \langle \exp(-i\mathbf{k} \cdot \mathbf{r}_i) | \hat{H} | \exp(-i\mathbf{k} \cdot \mathbf{r}_j) \rangle}{\sum_{i,j} c_i^* c_j \langle \exp(-i\mathbf{k} \cdot \mathbf{r}_i) | \exp(-i\mathbf{k} \cdot \mathbf{r}_j) \rangle}, \quad (2.18)$$

where λ and ϕ correspond to a different expectation value and the eigenfunction with the smallest eigenvalue, respectively. The smallest eigenvalue is correspond to the ground state.

2.3 Hartree-Fock Approximation

The main problem to solve the many-body Schrödinger equation is the representation of the many-body wavefunction. In 1928, Douglas Hartree developed approximation which is simplify the problem of electron-electron interactions by assuming the many-body electron wavefunction is expressed as a product of single electron wavefunction; this approximation is commonly recognized as a Hartree approximation[35]. Using this approximation and also involving the variation principle, we can solve the many-body Schrödinger equation as a N -single electrons system. The wavefunction for Hartree approximation can be expressed as follow:

$$\Psi_H(\mathbf{r}_1, \mathbf{r}_2, \dots, \mathbf{r}_N) = \frac{1}{\sqrt{N!}} \phi(\mathbf{r}_1), \phi(\mathbf{r}_2), \dots, \phi(\mathbf{r}_N), \quad (2.19)$$

where $\Psi_H(\mathbf{r}_i)$ consists of the spatial wavefunction ϕ_i .

However, in 1930, John Clarke Slater and Vladimir Aleksandrovich Fock independently proved that the Hatree approximation can not explain the principle of antisymmetry for the wavefunction of electrons[36-38]. The Hartree approximation does not consider the exchange interaction since Eq. (2.19) does not satisfy Pauli's exclusion principles. Then Slater introduced the determinant of many-body electrons which is satisfy the antisymmetry property and suitable for variation principles. Therefore, in 1935, Douglas Hatree reformulated the method and then recognized this as a Hatree-Fock (HF) approximation[39]. As already mentioned before that HF use Slater determinant which is can represent the N -electron wavefunctions as follow:

$$\Psi_{HF} = \frac{1}{\sqrt{N!}} \begin{vmatrix} \phi_1(\mathbf{r}_1) & \phi_2(\mathbf{r}_1) & \dots & \phi_N(\mathbf{r}_1) \\ \phi_1(\mathbf{r}_2) & \phi_2(\mathbf{r}_2) & \dots & \phi_N(\mathbf{r}_2) \\ \vdots & \vdots & \dots & \vdots \\ \phi_1(\mathbf{r}_N) & \phi_2(\mathbf{r}_N) & \dots & \phi_N(\mathbf{r}_N) \end{vmatrix} \quad (2.20)$$

with additional orthonormal constraint

$$\int \phi_i^*(\mathbf{r})\phi_j(\mathbf{r})d\mathbf{r} = \langle \phi_i | \phi_j \rangle \quad (2.21)$$

By using above Slater determinant, we can determine the HF energy from the expectation value of Hamiltonian, which is can be expressed as follow:

$$E = \langle \Psi_{HF} | \hat{H} | \Psi_{HF} \rangle = 2 \sum_i^N h_i + \sum_i^N \sum_i^N (2J_{i,j} - K_{i,j}). \quad (2.22)$$

The first term in Eq.(2.22) is represents the kinetic energy of electrons and the interaction between energy and nuclei. On the other hand, in second term is expresses the interaction between two electrons which is commonly recognized as a Coulomb interaction energy and also exchange integrals. The first and second term can be expanded as the expression as follow:

$$h_i = \int \phi_i^*(\mathbf{r}_1)\hat{h}\phi_i(\mathbf{r}_1)d\mathbf{r}_1, \quad (2.23)$$

$$J_{i,j} = \int \int \phi_i^*(\mathbf{r}_1)\phi_i(\mathbf{r}_1) \frac{1}{|\mathbf{r}_1 - \mathbf{r}_2|} \phi_j^*(\mathbf{r}_2)\phi_j(\mathbf{r}_2)d\mathbf{r}_1d\mathbf{r}_2, \quad (2.24)$$

$$K_{i,j} = \int \int \phi_i^*(\mathbf{r}_1)\phi_j(\mathbf{r}_1) \frac{1}{|\mathbf{r}_1 - \mathbf{r}_2|} \phi_j^*(\mathbf{r}_2)\phi_i(\mathbf{r}_2)d\mathbf{r}_1d\mathbf{r}_2. \quad (2.25)$$

The term $J_{i,j}$ and $K_{i,j}$ are commonly recognized as the Coulomb integral and the exchange integral, respectively. To explain simple way to solve many-body interaction by using HF approximation, then we can introduce which V_{HF} is considered as HF potential. This potential describe the repulsive interaction between one electron with the other $N - 1$ electrons in average, in which consists of \hat{J} and \hat{K} which are represent as a Coulomb and an exchange operator, respectively. Both operator can be expressed as follow:

$$\hat{J}\phi(\mathbf{r}) = \int d\mathbf{r}_2 \frac{|E_j(\mathbf{r}_2)|^2}{|\mathbf{r}_1 - \mathbf{r}_2|} E_i(\mathbf{r}_1), \quad (2.26)$$

$$\hat{K}\phi(\mathbf{r}) = \int d\mathbf{r}_2 \frac{E_j^*(\mathbf{r}_2)E_i(\mathbf{r}_2)}{|\mathbf{r}_1 - \mathbf{r}_2|} E_j(\mathbf{r}_1). \quad (2.27)$$

Then we conclude that the HF is constructed by the effective wavefunction and the effective potential. We give the initial input HF wavefunction which is corresponds to Slater determinant. After that, we construct the potential operator by considering the electron-electron interaction and also considering self interaction. Next

iteration is calculated based on the previous calculations until the convergence is achieved. This method commonly recognized as *self-consistent field* (scf)[36].

2.4 Density Functional Theory (DFT)

The main idea of Density Functional Theory (DFT) is represented the interacting system as an electron density instead of wavefunction. The electron density equation can be expressed as follow:

$$n(\mathbf{r}) = N \sum_{s_1} \cdots \sum_{s_N} \int \cdots \int |\Psi(\mathbf{r}_1, \mathbf{s}_1, \cdots, \mathbf{r}_N, \mathbf{s}_N)|^2 d\mathbf{r}_1 d\mathbf{r}_2 \cdots d\mathbf{r}_N, \quad (2.28)$$

and

$$\int n(\mathbf{r}) d\mathbf{r} = N. \quad (2.29)$$

The DFT construct by two fundamental theorems state by Walter Kohn and Pierre Hohenberg in 1964[40]. In the following subsections will be explained this two theorems and also the Kohn-Sham equation.

2.4.1 Hohenberg-Kohn Theorems

The work of Walter Kohn and Pierre Hohenberg can be summarized as two fundamentals theorem which is commonly recognized as the fundamentals concept of DFT. The first theorem as follow:

Theorem 2.1 (Hohenberg-Kohn I, 1964). *The ground state density $n(\mathbf{r})$ of many body quantum system in some external potential V_{ext} determines this potential uniquely.*

Proof: The first theorem can be proved by *reductio ad absurdum*. Let assume we have two different external potential; $V_{ext}^{(1)}$ and $V_{ext}^{(2)}$ in which have the same of ground state density $n_0(\mathbf{r})$. This two external potential have two different Hamiltonian for example $\hat{H}^{(1)}$ and $\hat{H}^{(2)}$, also they have two different ground state wavefunction such as $\psi^{(1)}$ and $\psi^{(2)}$. Hypothetically, this two wavefunction have the same ground state electron density $n_0(\mathbf{r})$ but different ground state of energy. Since $\psi^{(2)}$ correspond to $\hat{H}^{(2)}$ and it does not related with $\hat{H}^{(1)}$, therefore we can

obtain:

$$E^{(1)} = \langle \psi^{(1)} | \hat{H}^{(1)} | \psi^{(1)} \rangle < \langle \psi^{(2)} | \hat{H}^{(1)} | \psi^{(2)} \rangle. \quad (2.30)$$

The last term in Eq.(2.30) above can be expressed as follow:

$$\begin{aligned} \langle \psi^{(2)} | \hat{H}^{(1)} | \psi^{(2)} \rangle &= \langle \psi^{(2)} | \hat{H}^{(2)} | \psi^{(2)} \rangle + \langle \psi^{(2)} | \hat{H}^{(1)} - \hat{H}^{(2)} | \psi^{(2)} \rangle \\ &= E^{(2)} + \int d^3r [V_{ext}^{(1)}(\mathbf{r}) - V_{ext}^{(2)}(\mathbf{r})] n_0(\mathbf{r}), \end{aligned} \quad (2.31)$$

then we can obtain

$$E^{(1)} < E^{(2)} + \int d^3r [V_{ext}^{(1)}(\mathbf{r}) - V_{ext}^{(2)}(\mathbf{r})] n_0(\mathbf{r}). \quad (2.32)$$

Using the same method we can find similar expression like Eq.(2.32) for $E^{(2)}$, as below:

$$E^{(2)} < E^{(1)} - \int d^3r [V_{ext}^{(1)}(\mathbf{r}) - V_{ext}^{(2)}(\mathbf{r})] n_0(\mathbf{r}). \quad (2.33)$$

Then we add Eq. (2.32) and (2.33) than this summation obtain the inconsistency:

$$E^{(1)} + E^{(2)} < E^{(1)} + E^{(2)}. \quad (2.34)$$

Therefore this theorem has proven by *reductio ad absurdum*.

Theorem 2.2 (Hohenberg-Kohn II, 1964). *A universal functional for the energy $E[n]$ in terms of the density $n(\mathbf{r})$ can be defined, valid for any external potential $V_{ext}(\mathbf{r})$. For any particular $V_{ext}(\mathbf{r})$, the exact ground state energy of the system is the global minimum value of this functional and the density $n(\mathbf{r})$ that minimizes the functional is the exact ground state density $n_0(\mathbf{r})$.*

Proof: Since all properties can be seen as a functional of $n(\mathbf{r})$; including total energy functional, therefore we can obtain:

$$E_{HK}[n(\mathbf{r})] = T[n(\mathbf{r})] + E_{int}[n(\mathbf{r})] + \int V_{ext}(\mathbf{r})n(\mathbf{r})d^3\mathbf{r} + E_{NN} \quad (2.35)$$

where E_{NN} is the interaction energy between nuclei. We can express the kinetic and internal potential energies as a universal functional of the charge density $F[n(\mathbf{r})]$; due to the fact that both are the same for all system. Therefore we can write the Eq.(2.35) above as follow:

$$E_{HK}[n(\mathbf{r})] = F[n(\mathbf{r})] + \int V_{ext}(\mathbf{r})n(\mathbf{r})d^3\mathbf{r} + E_{NN} \quad (2.36)$$

Let assume we have ground state electron density $n^{(1)}(\mathbf{r})$ which is correspond V_{ext}^1 :

$$\begin{aligned} E^{(1)} &= E_{HK}[n^{(1)}(\mathbf{r})] \\ &= \langle \psi^{(1)} | \hat{H}^{(1)} | \psi^{(1)} \rangle. \end{aligned} \quad (2.37)$$

Then we introduce new electron density, $n^{(2)}(\mathbf{r})$; in which correspond to the wavefunction ψ_2 :

$$E^{(2)} = \langle \psi^{(2)} | \hat{H}^{(1)} | \psi^{(2)} \rangle. \quad (2.38)$$

From Eq.(2.37) and Eq.(2.38) we can obtain that:

$$\langle \psi^{(1)} | \hat{H}^{(1)} | \psi^{(1)} \rangle < \langle \psi^{(2)} | \hat{H}^{(1)} | \psi^{(2)} \rangle. \quad (2.39)$$

Then we can minimizing the energy $E^{(2)}$ with respect to electron density $n(\mathbf{r})$ and express the total energy as a function of electron density until obtain the ground state energy, which is correspond to the correct density minimizing the energy.

2.4.2 The Kohn-Sham Equation

The Kohn-Sham (KS) equation correspond to the concept introduced in 1965 by Walter Kohn and Lu Jeu Sham as the fundamental concept due to the application of DFT[41,42]. The KS uses the Hohenberg-Kohn theorem which has already explained in the previous subsection. The KS equation explain that the total energy of the system depends on the electron density of the system where this statement can be expressed as follow:

$$E = E[n(\mathbf{r})]. \quad (2.40)$$

The idea is mapping an interacting electrons system into an auxiliary system of a non-interacting electrons with the same ground state of electron density $n(\mathbf{r})$. For a system of non-interacting electrons, the ground state of electron density is represented as a sum of all electron orbitals which is can be expressed as follow:

$$n(\mathbf{r}) = \sum_i^N |\phi_i(\mathbf{r})|^2, \quad (2.41)$$

where i is calculated from 1 to $N/2$ if we consider double occupancy of all states and also we have to multiplied the sum by 2. The electron can be varied by

changing the trial wavefunction of the system. If the electron density correspond to the minimum energy, the whole system is a ground state. Therefore, by solving KS equation then we can find the ground state density and also ground state energy. The accuracy of the calculation results are depend on the exchange and the correlation interaction.

The KS approach replaces the interacting electron system into a non interacting case, in which we introduce the new potential, commonly is called effective potential. The effective potential consists of external potential, Coulomb interaction between electrons, the exchange interaction and correlation effect. Therefore, the KS equation can be expanded as follow:

$$E_{KS} = T[n(\mathbf{r})] + E_H[n(\mathbf{r})] + E_{XC}[n(\mathbf{r})] + \int d\mathbf{r} V_{ext} n(\mathbf{r}). \quad (2.42)$$

The first term in Eq. (2.42) represents the kinetic energy of a non-interacting electrons:

$$T[n(\mathbf{r})] = -\frac{\hbar^2}{2m} 2 \sum_i \Psi_i^*(\mathbf{r}) \nabla^2 \Psi_i(\mathbf{r}) d\mathbf{r}, \quad (2.43)$$

The second in Eq. (2.42) is correspond to the Hartree energy containing the electrostatic interaction between cloud of charge:

$$E_H[n(\mathbf{r})] = \frac{e^2}{2} \int \frac{n(\mathbf{r})n(\mathbf{r}')}{|\mathbf{r} - \mathbf{r}'|} d\mathbf{r}d\mathbf{r}'. \quad (2.44)$$

All effects related to exchange and correlation are grouped into exchange-correlation energy which commonly expressed as E_{XC} . Then, after we determine the E_{XC} part, we can find the ground state electron density and also the ground state of total energy in which represent the system.

We can solve KS equation by functional derivatives with respect to the electron density $n(\mathbf{r})$ as follow:

$$\begin{aligned} \frac{\delta E_{KS}}{\delta \Psi_i^*(\mathbf{r})} &= \frac{\delta T[n(\mathbf{r})]}{\delta \Psi_i^*(\mathbf{r})} + \left[\frac{\delta E_{ext}[n(\mathbf{r})]}{\delta n(\mathbf{r})} + \frac{\delta E_H[n(\mathbf{r})]}{\delta n(\mathbf{r})} + \frac{\delta E_{XC}[n(\mathbf{r})]}{\delta n(\mathbf{r})} \right] \frac{\delta n(\mathbf{r})}{\delta \Psi_i^*(\mathbf{r})} \\ &- \frac{\delta(\lambda \int n(\mathbf{r}) d\mathbf{r} - N)}{\delta n(\mathbf{r})} \left[\frac{\delta n(\mathbf{r})}{\delta \Psi_i^*(\mathbf{r})} \right] = 0, \end{aligned} \quad (2.45)$$

where λ correspond to Lagrange multiplier which is already mentioned in previous subsections, V_{XC} is the exchange and correlation potential where can be expressed

as below:

$$V_{XC} = \frac{\delta E_{XC}[n(\mathbf{r})]}{\delta n(\mathbf{r})}. \quad (2.46)$$

The last term is the Lagrange multiplier for handling the constraint, we get a non-trivial solution. The first, second and third terms in Eq. (2.45) are given by:

$$\frac{\delta T[n(\mathbf{r})]}{\delta \Psi_i^*(\mathbf{r})} = -\frac{\hbar^2}{2m} 2\nabla^2 \Psi_i(\mathbf{r}), \quad (2.47)$$

$$\left[\frac{\delta E_{ext}[n(\mathbf{r})]}{\delta n(\mathbf{r})} + \frac{\delta E_H[n(\mathbf{r})]}{\delta n(\mathbf{r})} + \frac{\delta E_{XC}[n(\mathbf{r})]}{\delta n(\mathbf{r})} \right] \frac{\delta n(\mathbf{r})}{\delta \Psi_i^*(\mathbf{r})} = 2(V_{ext}(\mathbf{r}) + V_H(\mathbf{r}) + V_{XC}(\mathbf{r})), \quad (2.48)$$

$$\frac{\delta(\lambda \int n(\mathbf{r}) d\mathbf{r} - N)}{\delta n(\mathbf{r})} \left[\frac{\delta n(\mathbf{r})}{\delta \Psi_i^*(\mathbf{r})} \right] = 2\epsilon_i \Psi_i(\mathbf{r}). \quad (2.49)$$

Inserting Eq. (2.47), (2.48) and (2.49) to Eq. (2.45), then we can prove that the Kohn-Sham equation reliable with the many body Schrodinger equation

$$\left[\frac{1}{2} \nabla^2 + V_{KS}(\mathbf{r}) \right] \Psi_i(\mathbf{r}) = \epsilon_i \Psi_i(\mathbf{r}), \quad (2.50)$$

where

$$V_{KS} = V_{ext}(\mathbf{r}) + V_H(\mathbf{r}) + V_{XC}(\mathbf{r}), \quad (2.51)$$

or

$$V_{KS} = V_{ext}(\mathbf{r}) + \frac{e^2}{2} \int \frac{n(\mathbf{r}')}{|\mathbf{r} - \mathbf{r}'|} d\mathbf{r}' + V_{XC}(\mathbf{r}). \quad (2.52)$$

If the independent-particle system has the same ground state as the real interacting system, then many-body electron problem can be reduced into one-electron problem. Therefore, we can write

$$V_{KS} = V_{eff}. \quad (2.53)$$

The kinetic energy $T[n(\mathbf{r})]$ is given by

$$T[n(\mathbf{r})] = \sum_i \epsilon_i - \int n(\mathbf{r}) V_{eff} d\mathbf{r}. \quad (2.54)$$

By substituting this formula in Eq. (2.42), then we can obtain the total energy given by:

$$E_{KS}[n(\mathbf{r})] = \sum_i \epsilon_i + \frac{1}{2} \int \frac{n(\mathbf{r})n(\mathbf{r}')}{|\mathbf{r} - \mathbf{r}'|} d\mathbf{r}d\mathbf{r}' + E_{XC}[n(\mathbf{r})] - \int n(\mathbf{r})V_{eff}d\mathbf{r}. \quad (2.55)$$

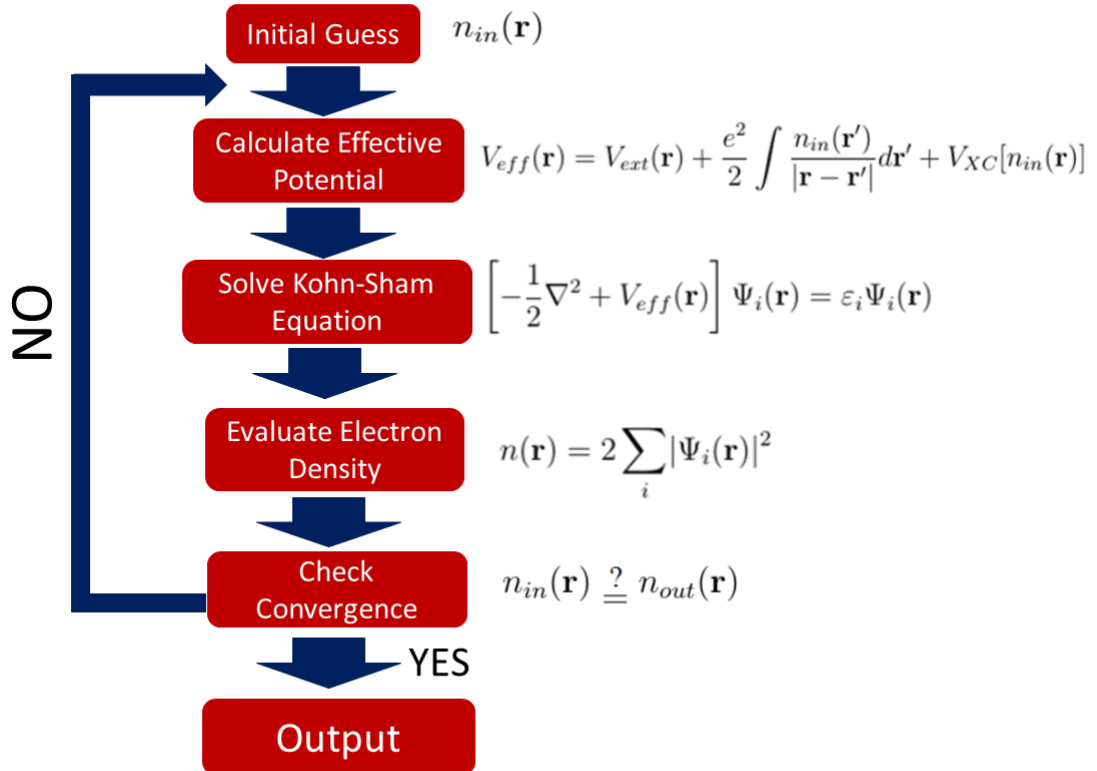


Figure 2.1: Self consistent scheme of Kohn-Sham equation.

Since the Hartree term and V_{XC} depend on $n(\mathbf{r})$, which is dependent on Ψ_i , the KS equation should be solved in an iterative self-consistent way. Starting from an initial guess for electron density $n(\mathbf{r})$ and then calculating the corresponding V_{XC} and V_H . The KS equation for the Ψ_i , can be solved by producing new electron density that will be used for new initial guess in the next interactive step. This procedure is repeated until the convergence is reached. This iterative procedure can be drawn as flow chart in Fig. (2.1).

2.5 Hubbard Model

In the case of strong electron-electron interactions, the average interaction energy becomes larger than the kinetic energy can give drastic changes of the properties of the system. The electrons have a tendency to localize which is to minimize their repulsion and also increase the kinetic energy[42]. Materials with this phenomena which play an important role for the electronic properties become the center of the research both in the theoretical study and experimental study for the last few decades. In this thesis we also explain that the origin of the negative value of FCIC is due to the existence of electron correlation phenomena in the anomalous muonium in silicon.

The method that is commonly used in the case of strong electron-electron interactions is a Hubbard model which is a tight-binding model with only one site interactions. We consider the system with a fixed lattice and nondegenerate band. In real space the model can be expressed as follows [43]:

$$H = -t \sum_{\langle i,j \rangle, \sigma} c_{i\sigma}^\dagger c_{j\sigma} + U \sum_i n_{i\uparrow} n_{i\downarrow}. \quad (2.56)$$

where $n_{i\sigma} = c_{i\sigma}^\dagger c_{i\sigma}$ and the summation in the first term goes over nearest neighbors $\langle i, j \rangle$. The negative sign in Eq. (2.56) is chosen for convenience because the bottom of the corresponding tight-binding band will be at $k = 0$. In more complicated cases the signs of different hopping matrix elements have to be fixed which is what can modify the results.

2.6 The Calculation Methods

2.6.1 Spin-polarized density functional calculations

First-principles calculations based on the spin-polarized density-functional theory are carried out by using PHASE/0 code[40,41,44,45]. In this calculation, we use a supercell approximation to study muonium in silicon crystals[22,46]. The norm-conserving pseudopotential developed by Troullier and Martins is used for both atoms[47]. We set the cut off energies 25 Rydberg and 100 Rydberg, respectively, for the wavefunctions and charge density. We use the local density

approximation (LDA) and the generalized gradient approximation (GGA) for the exchange-correlation energy. The LDA calculation is based on the method developed by Perdew and Wang[48] and we use the Perdew-Burke-Ernzerhof formalism for the GGA calculations[49].

The lattice parameter of the unit cell is set to be 5.431 Å which is deduced from experimental data[50-52]. We vary the size of the supercell, and then we check the convergence of the FCIC. We adopt the Γ k point sampling for supercell calculations. We optimize the atomic geometries and in the optimized geometry, the atomic forces are less than 10^{-3} Hartree/Bohr and the total energy is converged within 10^{-10} Hartree/cell. By using the k points of the $4 \times 4 \times 4$ mesh grid, we apply the tetrahedron method to the calculations of density of states (DOS) and projected density of states (PDOS).

2.6.2 Fermi contact interaction

The hamiltonian for the hyperfine interaction is expressed as:

$$\mathcal{H} = \mathbf{S}^e \mathbf{A} \mathbf{S}^I, \quad (2.57)$$

where $\mathbf{S}^e, \mathbf{S}^I$ and \mathbf{A} are electron spin, nuclear spin and hyperfine tensor, respectively. The hyperfine tensor consists of two parts, i.e., the isotropic part \mathbf{A}_s and anisotropic part \mathbf{A}_p . In this work, we focus on the isotropic part, which is expressed as:

$$\mathbf{A}_s = \frac{2\mu_0}{3} \hbar \gamma^e \gamma^I \rho_{spin}(0) \mathbf{1}, \quad (2.58)$$

where $\mathbf{1}$ is the 3×3 unit matrix. Equation (2.58) is expressed in the unit of MHz, where μ_0 ($4\pi \times 10^{-7} \text{ T}^2 \text{ m}^3 \text{ J}^{-1}$) is the permeability of vacuum, \hbar ($1.05457168(18) \times 10^{-34} \text{ J s}$) is the reduced Plank constant, γ^e ($1.76085974(15) \times 10^{11} \text{ T}^{-1} \text{ s}^{-1}$) is the electron gyromagnetic ratio and γ^I (133.81 MHz/T)³⁹⁾ is the gyromagnetic ratio of nucleus. The $\rho_{spin}(0)$ is the spin density of electron at the nuclear position. The isotropic part of hyperfine tensor can be expressed as follows:

$$\mathbf{A}_s = A_s \begin{pmatrix} 1 & 0 & 0 \\ 0 & 1 & 0 \\ 0 & 0 & 1 \end{pmatrix}, \quad (2.59)$$

where A_s in Eq.(2.59) is the FCIC. For the free atom, the FCIC is expressed as follows:

$$A_s^{free} = \frac{2\mu_0}{3} \hbar \gamma^e \gamma^I |\phi_s(0)|^2, \quad (2.60)$$

where $|\phi_s(0)|^2$ is the electron spin density at the free muonium site, which originates from the s orbital. Since the electron density is equal to $1/\pi$, the value of A_s^{free} is equal to 4472 MHz.

We follow the method by Van de Walle and Blöch to evaluate the FCIC by using the pseudopotential calculations. To evaluate $\rho_{spin}(0)$, we use the following approximation [19,30]:

$$\rho_{spin}(0) = \tilde{\rho}_{spin}(\vec{R}) \frac{|\phi_s(0)|^2}{|\tilde{\phi}_s(0)|^2}, \quad (2.61)$$

where $\tilde{\rho}_{spin}(0)$ is a pseudo-spin density at the muonium site and $|\tilde{\phi}_s(0)|^2$ is a pseudo-spin density of free muonium. Then the FCIC is given by[19,30]:

$$A_s = \frac{\tilde{\rho}_{spin}(0)}{|\tilde{\phi}_s(0)|^2} A_s^{free}. \quad (2.62)$$

To evaluate the reliability of the above approximation in the next section, we here introduce two quantities[19]:

$$\tilde{\eta} = \frac{\tilde{\rho}_{spin}(0)}{|\tilde{\phi}_s(0)|^2}, \quad (2.63)$$

where $\tilde{\eta}$ is the ratio of pseudo-spin density at the muonium site in silicon and pseudo-spin density of free muonium and

$$\eta = \frac{\rho_{spin}(0)}{|\phi_s(0)|^2}, \quad (2.64)$$

where η is the ratio of spin density at the muonium site in silicon from experimental data and spin density of free muonium.

Chapter 3

First-Principles Study of Anomalous Muonium in Silicon

3.1 Introduction

Muonium in silicon is one of the most extensively studied systems [18-34]. Theoretical calculations indicate that the muonium stopping site in silicon is the tetrahedral and bond-center sites; commonly recognized as normal muonium and anomalous muonium respectively. Anomalous muonium was detected and was clearly identified as the muonium located at the bond-center (BC) site, which is considered to be the most stable site [28](see Fig.(3.1)). This anomalous muonium was first time reported experimentally by *Patterson et al* [22]. They clarified that the muonium is located at [111] direction of silicon crystal, but the precise position was still unclear. Later the location was identified by *Kiefl et al* [25] who combined the level crossing resonance and μ SR methods. They confirmed that the muonium is located at the BC site by analyzing the HP, in particular FCIC.

The HP of anomalous muonium in silicon was calculated by several studies. Unfortunately, previous results largely deviated from the experimental data [19,22,25,30,33]. This discrepancy was possibility due to the small sizes of supercell used in previous reports. Therefore, in this study we consider to use large supercell to provide reliable calculation. Furthermore, the origin of the novel FCIC has not been clarified yet; the FCIC of the anomalous muonium is negative and the absolute value is extremely small.

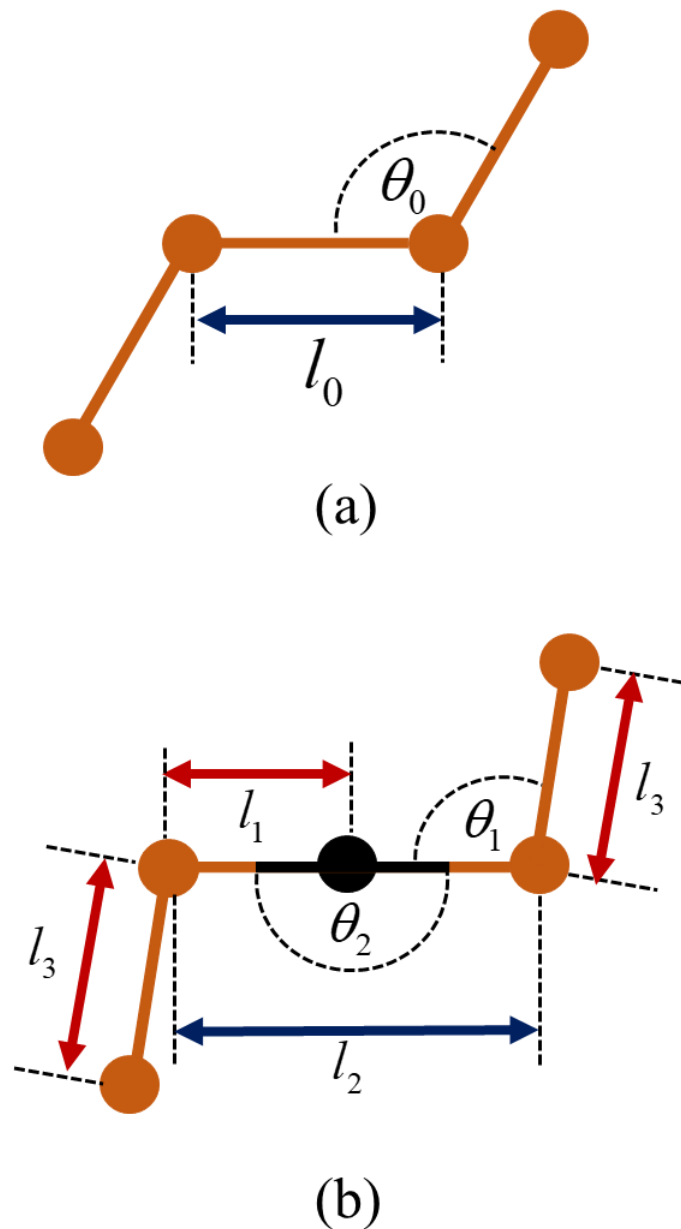


Figure 3.1: Geometries of pristine silicon (a) and muonium impurity at the BC site (b). $\theta_0 = 109.5^\circ$ and $l_0 = 2.35 \text{ \AA}$ respectively. The silicon and muonium atoms are denoted by the light brown sphere and black sphere, respectively.

In this chapter, we attempt to perform reliable first-principles calculations of the anomalous muonium. We perform spin polarized DFT calculations by using supercell models to simulate the impurity in silicon. It is found that we need to check the convergence of the supercell size; the conventionally used supercell sizes are found to be insufficient to get reliable results. We clarify the origin of the small absolute value of the FCIC and discuss its negative sign.

Table 3.1: Calculated geometry (angle) of the muonium impurity at the bond-centered (BC) site. The explanation of the geometrical parameters are given in Fig. 3.1.

Supercell size	Number of the silicon atoms	θ_1 (degree)		θ_2 (degree)	
		LDA	GGA	LDA	GGA
$2 \times 2 \times 2$	64	99.9	99.9	180	180
$3 \times 3 \times 3$	216	99.7	99.8	180	180
$4 \times 4 \times 4$	512	99.8	99.8	180	180
$5 \times 5 \times 5$	1000	99.9	99.9	180	180
$6 \times 6 \times 6$	1728	99.9	99.9	180	180

Table 3.2: Calculated geometry (distance between atoms) of the muonium impurity at the bond-centered (BC) site. The explanation of the geometrical parameters are given in Fig. 3.1.

Supercell size	Number of the silicon atoms	l_1 (Å)		l_2 (Å)		l_3 (Å)	
		LDA	GGA	LDA	GGA	LDA	GGA
$2 \times 2 \times 2$	64	1.619	1.619	3.238	3.237	2.312	2.313
$3 \times 3 \times 3$	216	1.624	1.619	3.247	3.239	2.320	2.321
$4 \times 4 \times 4$	512	1.614	1.614	3.228	3.227	2.322	2.322
$5 \times 5 \times 5$	1000	1.610	1.610	3.220	3.220	2.320	2.320
$6 \times 6 \times 6$	1728	1.607	1.606	3.214	3.212	2.320	2.320

3.2 Results and Discussion

We first determine the stable position of muonium and confirm that the BC site is the most stable. We carry out the calculation by moving the muonium slightly perpendicular from the BC site and set the minimum force as 10^{-3} Hartree/Bohr; as a result the muonium is located at the BC site in the optimized geometry. Figure 3.1 shows the geometry of the present system. Table 3.1 and 3.2 tabulate calculation results of the geometry of the muonium impurity at the BC site in silicon. We vary the size of supercell and find that the $4 \times 4 \times 4$ supercell gives a well converged result; the bond lengths are slightly varied within 0.01 \AA when we use the supercell of the $5 \times 5 \times 5$ and $6 \times 6 \times 6$ sizes. We confirm that the Si–Mu–Si bond is linear and the distance between the nearest two silicon atoms is 3.2 \AA . The distance between the first nearest and the second nearest host atoms is close to the bond length of the perfect crystal, i.e., the difference is within 0.001 \AA .

We next calculate the FCIC (Fig. 3.2(a) and 3.2(b)). The constant reaches the convergence by using the supercell of the $4 \times 4 \times 4$ size: the supercell gives the value close to those from the value from the $5 \times 5 \times 5$ and $6 \times 6 \times 6$ supercell calculations; the difference in the FCIC between $4 \times 4 \times 4$ and these two supercells is small (in

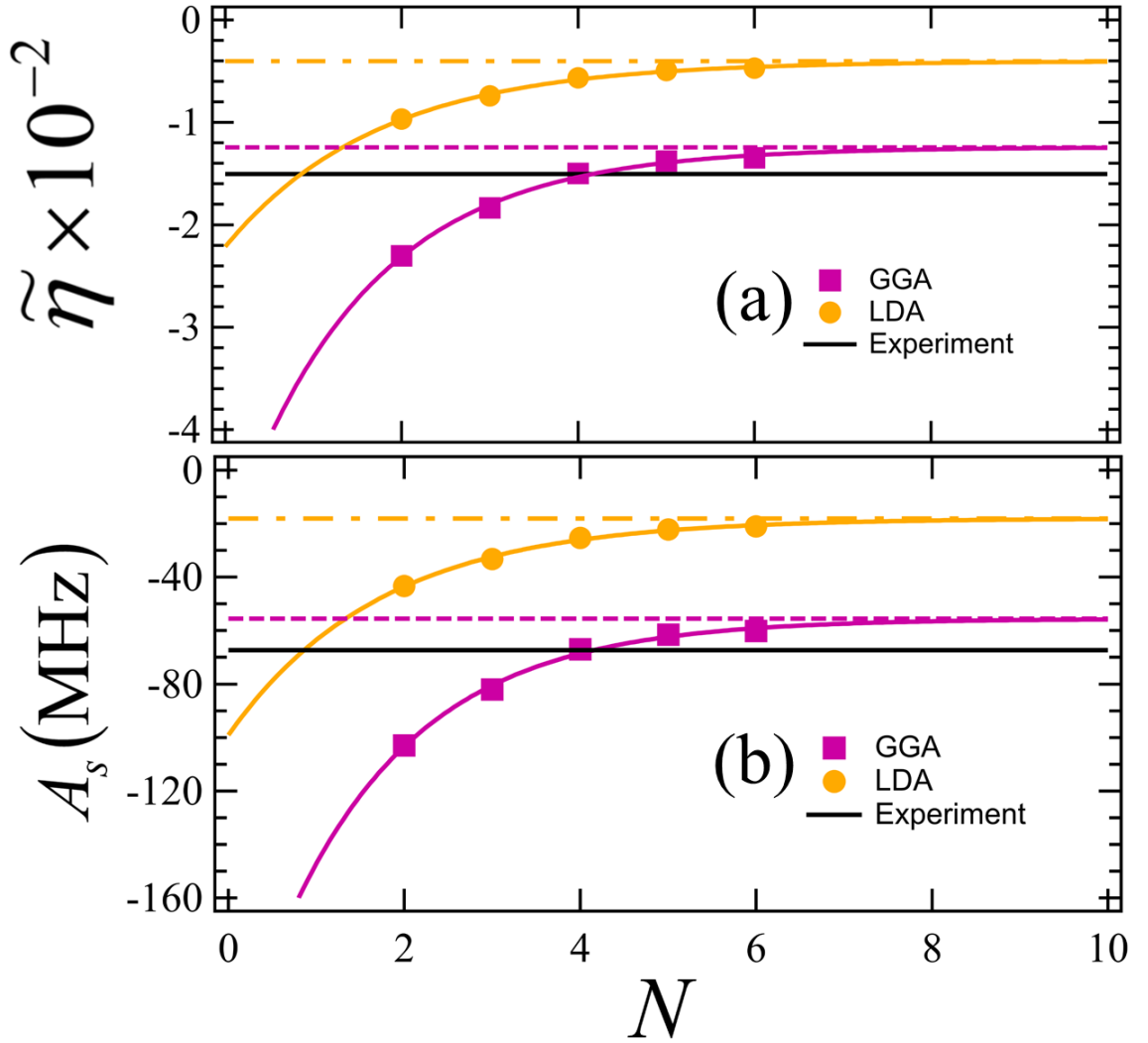


Figure 3.2: (a) Calculated $\tilde{\eta}$ given in Eq.(7). The black solid line represents η in Eq. (2.64) deduced from experimental data[25]. We present the fitting curves for the LDA and GGA calculational results. (b) Calculated FCIC. The experimental value is deduced from Ref. 25 and is represented by the black solid line. The horizontal axis represents N which means that the supercell size is $N \times N \times N$.

the case of the GGA calculation the differences are 5.5 MHz and 6.9 MHz for $5 \times 5 \times 5$ and $6 \times 6 \times 6$ supercells respectively). We find the deviations are following function well fits to the above mentioned FCIC

$$Y_{FCIC} = A + B \exp(-\alpha N), \quad (3.1)$$

where N is the supercell parameter, which means that the supercell size is $N \times N \times N$. We find that the converged values for the GGA and LDA are -55.6 MHz and -18.0 MHz, respectively. The determined value of A , B , and α are tabulated

in Table 3.3.

Table 3.3: Fitting parameters in Eq. (3.1) and Eq. (3.2)

Exchange Energy	$A(\text{MHz})$	$B(\text{MHz})$	α	A'	B'	α'
GGA	-55.6	-175.6	0.65	-0.012	-0.039	0.651
LDA	-18.0	-81.1	0.57	-0.004	-0.018	0.577

Table 3.4: FCIC of muonium at the BC site. We show our calculational results for the 512, 1000, 1728 supercells and the value of FCIC from fitting is estimated by using Eq. (3.1).

References	Method	Exchange energy	Number of silicon atoms	FCIC (MHz)
Present	Pseudopotential	GGA	512	-67.1
Present	Pseudopotential	GGA	1000	-61.6
Present	Pseudopotential	GGA	1728	-60.2
Present(Fitting)	Pseudopotential	GGA		-55.6
Porter et.al[33]	All electron	GGA	16	-89.3
Porter et.al[33]	All electron	LDA	16	-27.1
Luchsinger et.al[30]	Pseudopotential	GGA	64	-81
Luchsinger et.al[30]	Pseudopotential	LDA	64	-26
Van de Walle and Blöchl[19]	Pseudopotential	LDA	32	-35
Experiment[25]				-67.3

The value calculated from the GGA calculation is found to be close to the experimental value [25]. The deviation of the above-mentioned converged value from the experimental one is 11.7 MHz (17.4%). This deviation is, in general, smaller than those in previous calculations (Table 3.4). The deviations are 22.0 MHz-41.3 MHz (33%-61%). One of the reasons for the discrepancy between the experimental and calculational results in the past studies is expected to be due to the fact that small sizes of supercells were used.

We also evaluate the value of $\tilde{\eta}$ in Eq. (2.63) from calculational results and introduce the following fitting expression which is similar to Eq. (3.1):

$$Y_{\tilde{\eta}} = A' + B' \exp(-\alpha' N). \quad (3.2)$$

The determined parameters are tabulate in Table 3.3. The converged value, A' (-0.012), is close to the value of η (-0.015) in Eq. (2.64) deduced from experimental

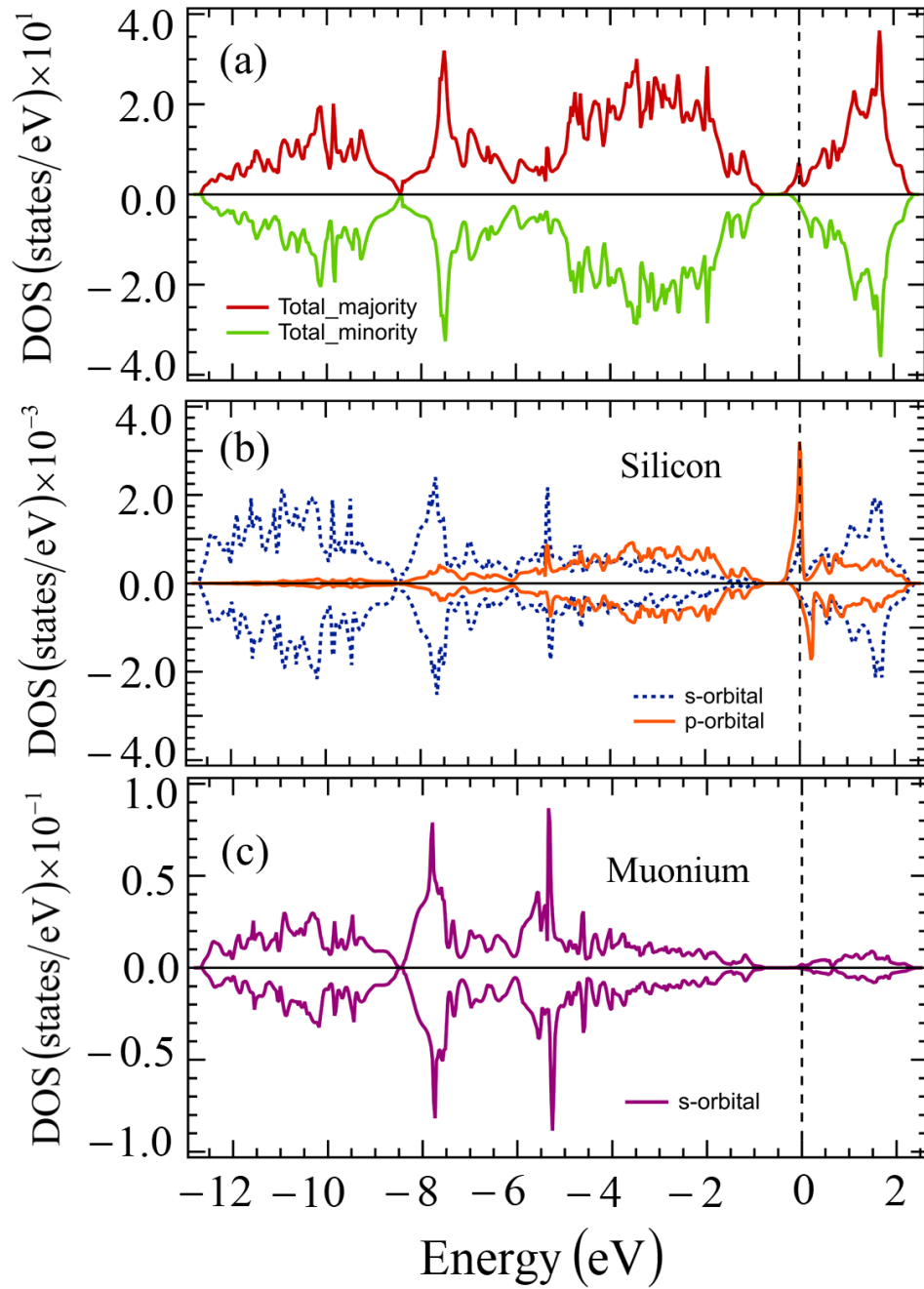


Figure 3.3: DOS (a) and PDOS of the nearest silicon atoms (b) and of the muonium (c). The vertical dashed lines indicate the Fermi level in the supercell calculations.

data (Fig. 3.2). This result suggests the validity of the approximation mentioned in the previous section which was introduced in Ref. 19 and Ref. 29.

We here calculate the DOS, PDOS (Fig. 3.3) and spin density (Fig. 3.4(a)). As the DOS (Fig. 3.3(a)) shows, the spin density mainly originates from the spin polarized impurity level which is located below the conduction band bottom. By

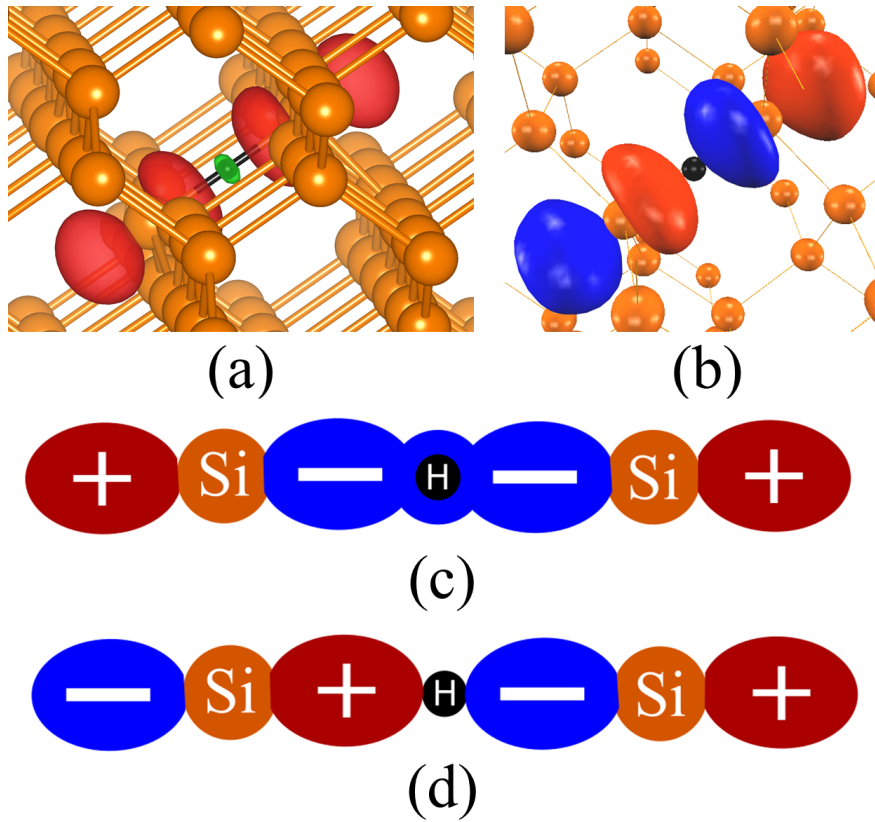


Figure 3.4: (a) Spin density where the absolute value of the isosurfaces is $1.50 \times 10^{-3} \text{ bohr}^{-3}$. The positive and negative spin densities are represented by red and green colors, respectively. The spin density was drawn using VESTA [54,55]. (b) Wavefunction of the impurity level. The red and blue colors represent positive and negative values, respectively. (c and d) Schematic view of two muonium related wavefunctions. The red and the blue colors represent the positive and negative values, respectively.

analyzing PDOS (Figs. 3.3(b) and 3.3(c)), we find that the impurity level mainly consists of the s and p orbitals of the nearest Si atoms and do not include the muonium s orbital component. As a result, the spin density is mainly distributed at the nearest two Si sites and the spin density is very small at the muonium site (Fig. 3.4(a)). This is the reason why the absolute value of FCIC is very small in this system: The observed FCIC of the anomalous muonium is -67.3 MHz[25], whose magnitude is much smaller than that of the free muonium (4463 MHz)[46].

Our calculation shows that the FCIC is negative, which is due to the fact that the spin density at the muon site is negative. We here discuss the origin of this negative spin density at the muon site. As was mentioned above, the impurity level does not contribute to the spin density at the muon site. Therefore, the spin density at the muon site is expected to originate from muon related states which are embedded in the valence band. Actually, the PDOS of the muon s orbital shows

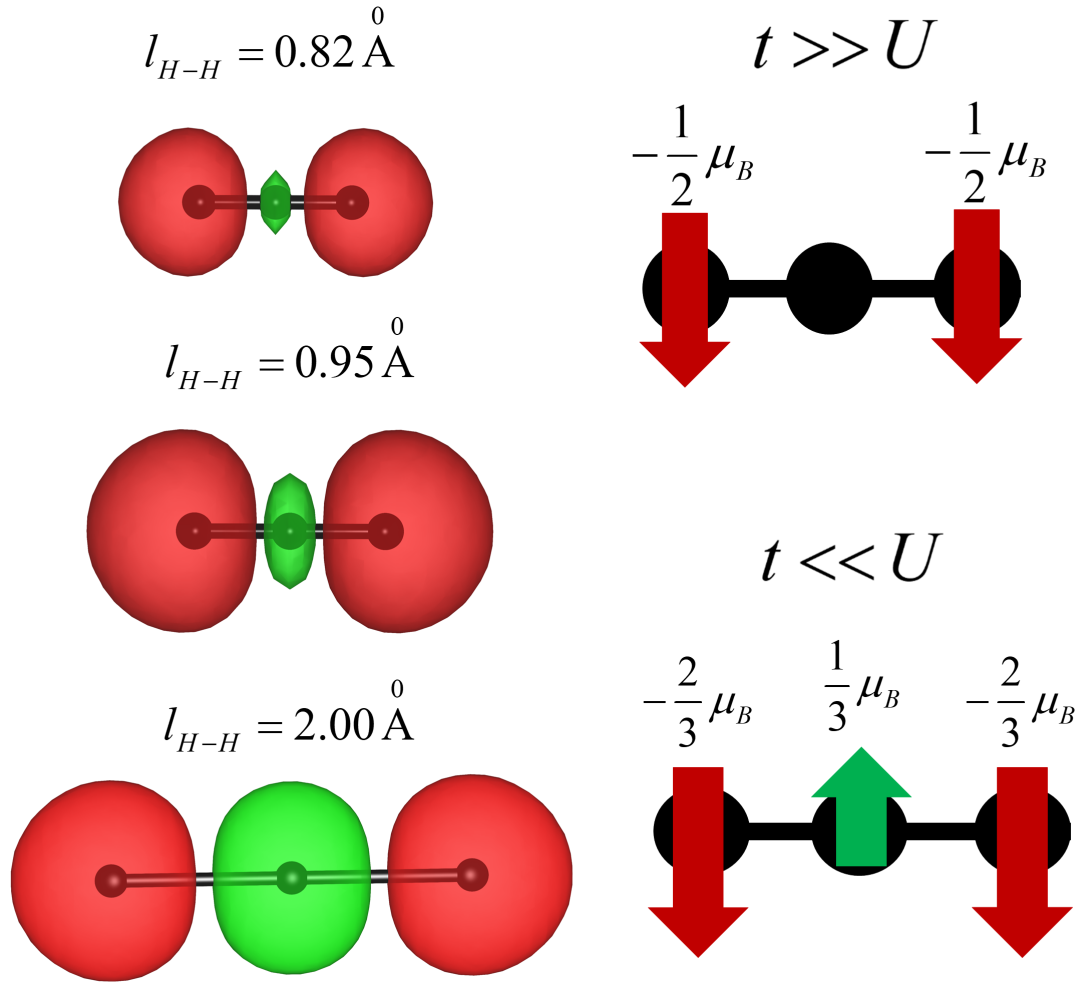


Figure 3.5: Spin densities of the linear tri-hydrogen molecule (the red and the green colors represent positive and negative value of isosurfaces, respectively) for the cases of $l_{H-H} = 0.82 \text{ \AA}$ (the isosurface value is $9.11 \times 10^{-2} \text{ spin/bohr}^{-3}$), $l_{H-H} = 0.95 \text{ \AA}$ (the isosurface value is $4.11 \times 10^{-2} \text{ spin/bohr}^{-3}$), and $l_{H-H} = 2.0 \text{ \AA}$ (the isosurface value is $4.11 \times 10^{-2} \text{ spin/bohr}^{-3}$). We also show the magnetic moment at each site calculated based on the Hubbard model. Two limiting cases ($t \gg U$ and $t \ll U$) are considered.

two strong peaks around -4 eV and -8 eV (Fig. 3.3(c)). The minority spin DOS at these peaks are found to be larger than those of the majority spin DOS. This difference causes the negative spin density at the muonium site.

We here introduce a simplified model to explain the above results concerning the negative spin density. In Fig. 3.4, we consider two wavefunctions. In the wavefunction in Fig. 3.4(c), the nearest Si orbitals and muonium s orbital have the same phases (bonding) and it is embedded in the deep of valence band. In the other wavefunction in Fig. 3.4(b) (schematic view is showed in Fig. 3.4(d)), the

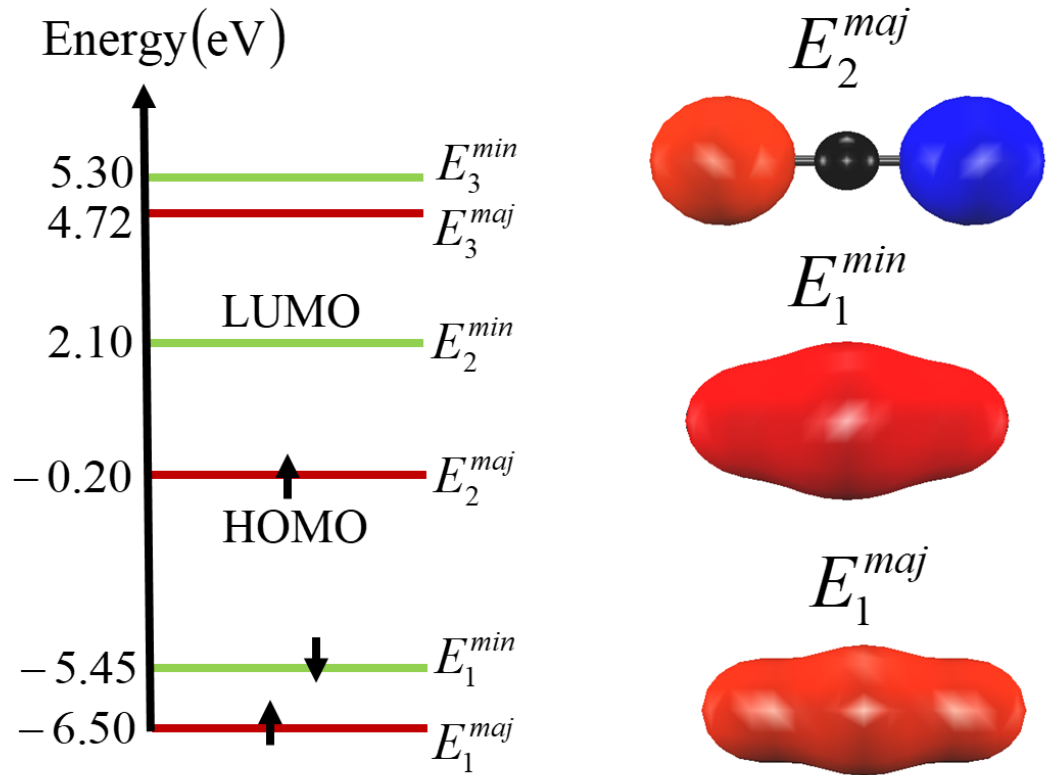


Figure 3.6: Schematic diagram of energies of the linear tri-hydrogen molecule on the lefthand side and wavefunctions on the righthand side where the red and blue colors represent positive and negative amplitudes, respectively.

two Si p orbitals have anti-phase, therefore there is a node at the muonium site. Since the former wavefunction has a relatively low energy and it has an amplitude at the muonium site, it contributes to the small but finite value of the FCIC. On the other hand, since the latter wavefunction has a relatively higher energy, it is included in the impurity level (Fig. 3.4(b)) and does not contribute to the FCIC.

To clearly understand the novel FCIC, we here introduce the linear tri-hydrogen molecule, which is considered to be a simplified model of the present system (Fig. 3.5). First, we consider a tight binding model including a hopping parameter t between the nearest atomic sites. Two electrons having majority and minority spins occupy the lowest energy level, $\phi_1 = \frac{1}{2}(\chi_1 + \sqrt{2}\chi_2 + \chi_3)$, where χ_1 and χ_3 are the atomic orbitals at the two side sites and χ_2 is the orbital at the middle site. This wavefunction corresponds to that in Fig. 3.4(c). A single majority spin electron occupies the second lowest level, $\phi_2 = \frac{1}{\sqrt{2}}(\chi_1 - \chi_3)$, which corresponds to that in Fig. 3.4(d). Therefore, the tight binding approximation leads to the result

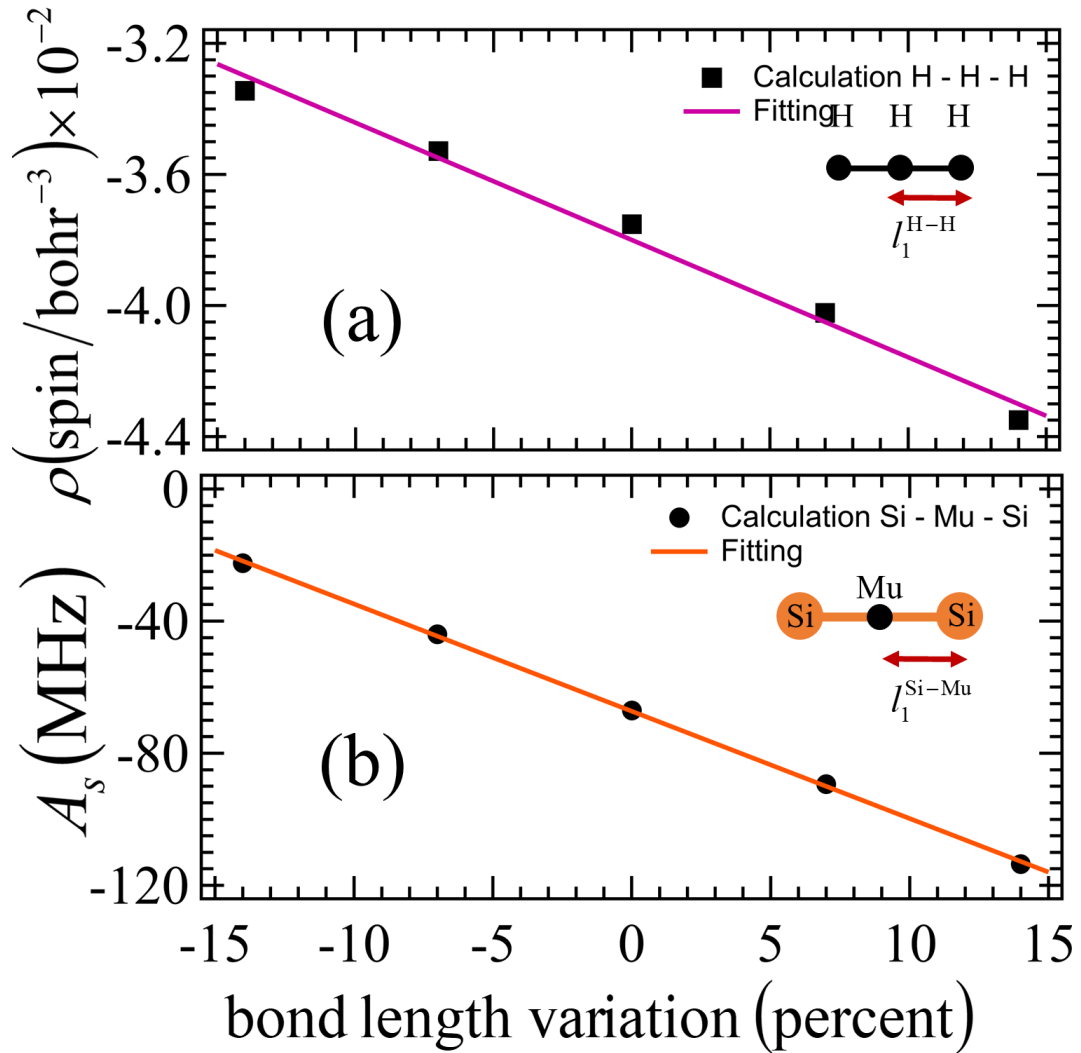


Figure 3.7: (a) Spin density of the linear tri-hydrogen molecule. We carry out calculations by changing the bond length from the equilibrium bond length ($l_{\text{H-H}}=0.95 \text{ \AA}$) (b) FCIC of anomalous muonium in silicon. The calculations are performed by changing the bond length from the equilibrium one ($l_{\text{Si-Mu}}=1.61 \text{ \AA}$).

that the spin density at the middle site is zero and the spin density appears at the both side sites (Each side site has the magnetic moment of $0.5 \mu_B$ and the middle site has no magnetic moment) (see Fig. 3.5).

We perform a GGA calculation on the linear tri-hydrogen molecule by taking the equilibrium bond length ($l_{\text{H-H}}=0.95 \text{ \AA}$) and obtain results which are similar to those based on the tight binding model; as Fig. 3.6 shows, low energy levels occupied by majority and minority spin electrons have wavefunctions similar to ϕ_1 and a high energy level occupied by a single majority spin electron has a wavefunction similar to ϕ_2 . However, there is a slight difference between the ϕ_1

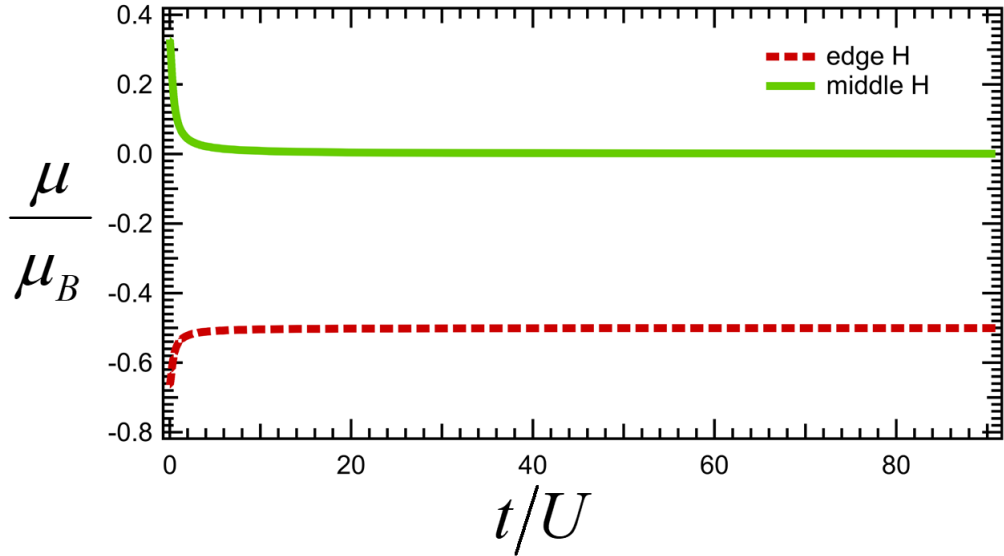


Figure 3.8: The magnetic moment of electrons based on the Hubbard model of three linear hydrogen molecule.

type wavefunctions occupied by majority spin and minority spin electrons. As a result, the middle site has a small amount of the spin density which is negative. This small value of the spin density cannot be explained based on the tight binding model which leads to the zero value of the spin density, so we expect that the nonzero value originates from the electron correlation effect.

We hence introduce the Hubbard model including the on-site Coulomb repulsion U as well as t [43]. We numerically solve the Hubbard model in the case of $\frac{t}{U} \rightarrow 0$, and find that the magnetic moments at the middle site and the side sites have the opposite signs; The magnetic moment at the middle site and the edge sites are $\frac{1}{3}\mu_B$ and $-\frac{2}{3}\mu_B$, respectively (see Fig. 3.5 and Fig. 3.8), which means that the spin density at the middle site is negative. We perform GGA calculation by taking a large bond length ($l_{H-H} = 2.0 \text{ \AA}$), which corresponds to a small $\frac{t}{U}$ case in the Hubbard model (see Fig. 3.5). The calculated spin density distribution is similar to that in the Hubbard model in the limit, $\frac{t}{U} \rightarrow 0$.

As $\frac{t}{U}$ becomes large, the magnitude of the spin density at the middle site is expected to decrease and get close to zero as is expected based on the tight binding model. This tendency of the spin density expected based on the Hubbard model is reproduced by our GGA calculation. We perform calculations for the bond lengths of 0.82 \AA , 0.95 \AA and 2.00 \AA and find that the magnitude of the spin density at the middle site becomes small as the bond length decreases (Fig. 3.5). This tendency of the spin density is also demonstrated in Fig. 3.7(a): We plot the spin densities

by varying the bond lengths around the equilibrium length (0.95 Å). The magnitude of the negative spin density linearly decreases as the bond length becomes small. Since a shorter bond corresponds to a larger t , the above mentioned results calculated based on the GGA are consistent with those based on the Hubbard model. We conclude that the negative spin density at the middle site is due to the electron correlation effect since it arises when U is not zero.

The spin density distribution in muonium in silicon is expected to be similar to that of the linear tri-hydrogen molecule where the two nearest Si atoms in the present system are substituted by hydrogen atoms. To confirm this expectation, we perform GGA calculations for various Si–Mu bond lengths; we displace the nearest two Si atoms from the equilibrium positions. As a result, we find that the magnitude of the negative FCIC becomes large as the Si–Mu bond length increases (Fig. 3.7(b)). This bond-length dependence of the FCIC is similar to that in the case of the spin density at the middle site in linear tri-hydrogen molecules. We expect that small magnitude of the FCIC corresponds to the case of a large $\frac{t}{U}$ in the Hubbard model for the linear tri-hydrogen molecule. It is noted, however, that the present Si–Mu bonds are resonant and thus the length (1.619 Å) is much longer than the conventional Si–Mu bond length; for example, the silane (SiH_4) forms the bonds whose lengths are 1.481 Å[53]). This rather long bond length is expected to enhance the magnitude of the FCIC compared with the cases of shorter bond lengths. Finally, by considering the analogy between the linear tri-hydrogen molecule and the present system, we attribute the negative FCIC to the electron correlation effect.

Chapter 4

Summary

4.1 Conclusion

We have carried out the first-principles calculation of the electronic structure of muonium in silicon using DFT, in particular anomalous muonium. We successfully reproduce the value of FCIC which is reliable with the experimental data and also we obtain convergence results. This convergence result can be obtained due to variation of the sizes of supercells. Our calculation shows that the FCIC is negative which corresponds to the spin density at muon site is negative. The impurity level does not contribute to the spin density at muon site. Therefore, the spin density at muon site is solely expected to originate from muon related states which are embedded in the valence band. In the PDOS of the muon s-orbital shows two strong peaks around -4 eV and -8 eV and the minority spin PDOS are found to be larger than those of the majority spin PDOS. We have clarified the origin of the very small magnitude and the origin of the negative value of FCIC. By considering the analogy between the three linear hydrogen molecule and the anomalous muonium in silicon, we concluded that the negative value is induced by the electron correlation effect.

4.2 Future Scope

We have successfully calculated anomalous muonium in silicon by using DFT. In this paper we also explain the origin of the small magnitude and the negative

value of FCIC in the case of anomalous muonium, which is considered as electron correlation effect. We already proven that DFT calculation is reliable for study of muonium in materials. Therefore we can extend our study about muonium to studies of other materials such as in a other semiconductors; perovskite, and gallium arsenide. In some semiconductors such gallium nitride and zinc oxide, muonium or hydrogen can behave as a shallow impurities[56]. Therefore, the study of FCIC of muonium as shallow impurities in semiconductors is really challenging which is also has not explained yet. The study of muonium in magnetic materials and strong correlated system has been attracted in the last few decades. DFT can be promising tool for study of this type materials.

The other methods also can be implemented due to the study of muonium. One of promising tool is Full Potential Linearized Augmented Planewave (FLAPW) method. This method enables all-electron calculations. Therefore, the calculation using FLAPW is promising method to study muonium accurately.

Bibliography

- [1] H. Amano, N. Sawaki and I. Akasaki and Y. Toyoda, Appl. Phys. Lett. **48**, 353 (1986)
- [2] H. Amano, M. Kito, K. Hiramatsu and I. Akasaki, Jpn. J. Appl. Phys. **28**, L2112 (1991)
- [3] S. Nakamura, T. Mukai and M. Senoh, Jpn. J. Appl. Phys. **30**, L1998 (1991)
- [4] S. Nakamura, Jpn. J. Appl. Phys. **30**, L1705 (1991)
- [5] S. Nakamura, Y. Harada, M. Senoh, Appl. Phys. Lett. **58**, 2021 (1991)
- [6] S. Nakamura, M. Senoh and T. Mukai, Appl. Phys. Lett. **62**, 2390 (1993)
- [7] S. Nakamura, M. Senoh, S. Nagahama, N. Iwasa, T. Yamada, T. Matsushita, H. Kiyoku and Y. Sugimoto Jpn. J. Appl. Phys. **35**, L74 (1996)
- [8] <https://www.nobelprize.org/>
- [9] M. Riordan, L. Hoddeson, and C. Herring, Rev. Mod. Phys. **71**, S336 (1999)
- [10] Hydrogen in Semiconductors, edited by J. Pankove and N.M. Johnson (Academic, New York, 1991)
- [11] H.J. Queisser and E.E. Haller, Science **281**, 945 (1998)
- [12] K. Shimomura, R. Kadono, K. Ohishi, M. Mizuta, M. Saito, K.H. Chow, B. Hitti and R.L. Lichti, Phys.Rev.Lett. **92**, 135505 (2004)
- [13] K. Shimomura *et.al.*, Physica B **376 – 377**, 444 (2006)
- [14] B. Monemar, P.P. Paskov, J.P. Bergman, M. Iwaya, S. Kamiyama, H. Amano and I. Akasaki, Physica B **376 – 377**, 460 (2006)

-
- [15] L.C.L. Hollenberg, A.S. Dzurak, C. Wellard, A.R. Hamilton, D.J. Reilly, G.J. Milburn and R.G. Clark, *Phys. Rev. B* **69**, 113301 (2004)
- [16] L.C.L. Hollenberg, A.D. Greentree, A.G. Fowler and C.J. Wellard, *Phys. Rev. B* **74**, 045311 (2006)
- [17] R.L. Lichti, *Protons and Muons in Materials Science*, edited by E.A. Davies and S.F.J. Cox (Taylor and Francis, London, 1996).
- [18] B.D. Patterson, *Rev.Mod. Phys.* **60**, 69 (1988)
- [19] C.G. Van de Walle and P.E. Blöchl, *Phys.Rev.B* **47**, 4244 (1993).
- [20] Yu. V. Gorelkinskii and N. N. Nevinnii, *Pi'sma Zh. Tekh. Fiz.* **13**, 105 (1987)[*Sov.Tech.Phys.Lett.* **13**, 45 (1987)].
- [21] K.M. Crowe, R.F. Johnson, J.H. Brewer, F.N. Gygax, D.G. Fleming and A. Schenck, *Bull. Am. Phys. Soc.* **17**, 594 (1972).
- [22] B.D. Patterson *et.al.*, *Phys.Rev.Lett.* **40**, 1347 (1978).
- [23] J.S. Wang and C. Kittel, *Phys.Rev.B* **7**, 713 (1973).
- [24] J.H. Brewer *et.al.*, *Phys.Rev.Lett.* **31**, 143 (1973).
- [25] R.F. Kiefl, M. Celio, T.L. Estle, S.R. Kretzman, G.M. Luke, T.M. Riseman and E.J. Ansaldo, *Phys.Rev.Lett.* **60**, 224 (1988).
- [26] S.F.J. Cox and M.C.R. Symon, *Chem.Phys.Lett.* **126**, 516 (1986).
- [27] D.M. Maric, S. Vogel, P.F. Meier and S.K. Estreicher, *Hyperfine Interact.* **64**, 573 (1990).
- [28] P.R. Briddon and R. Jones, *Hyperfine Interact.* **64**, 593 (1990).
- [29] C.G. Van de Walle, *Phys.Rev.Lett.* **64**, 669 (1990).
- [30] R.H. Luchsinger, Y. Zhou and P. Meier, *Phys.Rev.B* **55**, 6927 (1997).
- [31] T. Miyake, T. Ogitsu and S. Tsuneyuki, *Phys.Rev.Lett.* **81**, 1873 (1998).
- [32] T. Miyake, T. Ogitsu and S. Tsuneyuki, *Phys.Rev.B* **60**, 14197 (1999).
- [33] A.R. Porter, M.D. Towler and R.J. Needs, *Phys.Rev.B* **60**, 13534 (1999).
- [34] L. Liborio, S. Sturniolo and D. Jochym, *J. Chem. Phys.* **148**, 134114 (2018).

-
- [35] D.R. Hatree, Math. Proc. Camb. Philos. Soc. **24**, 111 (1928)
- [36] J.C. Slater, Phys. Rev. **32**, 339 (1928)
- [37] J.C. Slater, Phys. Rev. **35**, 210 (1930)
- [38] V.A. Fock, Z. Phys. **61**, 126 (1930)
- [39] D.R. Hatree and W Hatree, Proc. Royal Soc. Lond. A. **150**, 869 (1935)
- [40] P. Hohenberg and W. Kohn, Phys. Rev. **136**, B864 (1964)
- [41] W. Kohn and L.J. Sham, Phys. Rev. **140**, A1133 (1965)
- [42] D.I. Khomskii, Basic Aspect of Quantum Theory of Solids (Cambridge University Press, 2010)
- [43] J. Hubbard, Proc R Soc Lond. **276**, 1365 (1963)
- [44] M.C. Payne, M.P. Teter, D.C. Allan, T.A. Arias, J.D. Joannopoulos, Rev. Mod. Phys. **64** 1045 (1992)
- [45] <https://azuma.nims.go.jp/>
- [46] J.S. Möller, D. Ceresoli, T. Lancaster, N. Marzari and S.J. Blundell, Phys.Rev.B **87**, 121108(R) (2013)
- [47] N. Troullier and J.L. Martins, Phys.Rev.B **43**, 1993 (1991)
- [48] J.P. Perdew and Y. Wang, Phys.Rev.B **45**, 13244 (1992)
- [49] J.P. Perdew, K. Burke and M. Ernzerhof, Phys.Rev.Lett. **77**, 3865 (1996)
- [50] <https://crystdb.nims.go.jp/>
- [51] Y. Miyamoto and M. Hirata, J. Phys. Soc. Jpn. **44**, 181 (1978).
- [52] Y. Okada and Y. Tokumaru, J.Appl. Phys. **56**, 314 (1984).
- [53] A.F. Holleman E. Wiberg, Inorganic Chemistry (Academic Press, London, 2001)
- [54] <http://jp-minerals.org/vesta>
- [55] K. Momma and F. Izumi, J. Appl. Crystallogr. **44**, 1272 (2011).
- [56] T. Yamamoto, T. Uda, T. Yamasaki and T. Ohno, Phys. Lett A **373**, 3989 (2009).